

Semiclassical theory for the orbital magnetic moment of superconducting quasiparticles

Jian-hua Zeng,¹ Zhongbo Yan,^{1,2} Zhi Wang,^{1,2,*} and Qian Niu³

¹*School of Physics, Sun Yat-sen University, Guangzhou 510275, China*

²*Guangdong Provincial Key Laboratory of Magnetoelectric Physics and Devices,
Sun Yat-sen University, Guangzhou 510275, People's Republic of China*

³*Department of Physics, University of Science and Technology, Anhui, China*

We study the orbital magnetic moment of Bogoliubov quasiparticles in superconductors with the semiclassical approach. We derive the orbital magnetic moment of a quasiparticle wavepacket by considering the energy correction of the wavepacket to the linear order of the magnetic field. The semiclassical result is further verified by a linear response calculation with a full quantum mechanical method. From the analytical expression we find that nontrivial structure in the superconducting pairing gap alone is unable to produce quasiparticle orbital magnetic moment, which is in sharp contrast to the behavior of quasiparticle Berry curvatures. We apply the formula to study a tight-binding model with chiral d -wave superconducting gap, and show the influence of orbital magnetic moment on the energy spectrum and local density of states. We also calculate the orbital Nernst effect driven by the interplay between the orbital magnetic moment and the Berry curvature of Bogoliubov quasiparticles.

I. INTRODUCTION

Orbital magnetic moment plays an important role in the magnetic and optical properties of Bloch electrons [1–4]. The modern understanding of the orbital magnetic moment for Bloch electrons was formulated by several distinct methods such as the Wannier function approach [5, 6], the linear response approach [7], and the semiclassical approach [8, 9]. In the semiclassical picture, the orbital magnetic moment of Bloch electrons originates from the self-rotation of the wavepackets [10–12]. It is a crucial part of the orbital magnetization of the electron system [8, 9], which might be even larger than spin-induced magnetization. The orbital magnetic moment is also directly linked to various magnetic phenomena such as magnetoresistivity [13–15], Zeeman splitting [16–18], gyrotropic magnetic effect [19, 20], and magnetic susceptibility [21]. Furthermore, the orbital magnetic moment plays a pivotal role in transport phenomena, such as the nonlinear thermoelectric Hall effect [22, 23], the valley Hall effect [24–26], and the orbital Hall effect [27–33].

In superconducting systems, Bogoliubov quasiparticles behave similarly to Bloch electrons with a band structure determined by the Bogoliubov-de Gennes (BdG) Hamiltonian [34]. Since the BdG Hamiltonian is constructed by both the electron Hamiltonian and the superconducting gap function, the structure of the quasiparticle band is shaped by the interplay of the electron Bloch functions and the superconducting gap symmetry [35–37]. This interplay induces rich topological phases which support exotic boundary modes such as the chiral Majorana mode [35–37]. Meanwhile, the quasiparticle band structure also exhibits nontrivial geometric properties such as Berry curvatures [38–46], which can induce an anomalous Hall response for quasiparticles even in the topological trivial state [44].

From the perspective of BdG band, the orbital magnetic moment of superconducting quasiparticles obviously deserves

closer investigation. It has already drawn theoretical interest [47–50]. With a Wannier function approach, the orbital angular momentum of superconducting quasiparticles has been derived [47, 48], and the resulting orbital magnetization is decomposed into local and itinerant contributions. The orbital magnetic moment is also discussed from the perspective of conserved charge current in superconductors [49]. Linear response approach has also been taken to investigate the orbital magnetization and calculate various effects such as the orbital Edelstein effect [50–52]. Unlike the Bloch electrons, different methods for studying the orbital magnetic moment of superconducting quasiparticles often lead different results. The main difficulty lies in the charge non-conservation of mean-field BdG Hamiltonian, which brings a discrepancy between the charge distribution and the probability distribution of a quasiparticle wavepacket. This induces a subtle distinction between the orbital magnetic moment and the orbital angular momentum of superconducting quasiparticles.

Motivated by this theoretical gap, we provide a derivation of the orbital magnetic moment of Bogoliubov quasiparticles with a semiclassical approach. For this purpose we construct a quasiparticle wavepacket with the eigenstates of the BdG Hamiltonian, and calculate the gradient correction to the energy of the wavepacket with respect to the magnetic field. Following the protocol for treating Bloch electrons [10–12], we define the coefficient of the energy correction with respect to a homogeneous magnetic field as the orbital magnetic moment of the quasiparticle, and find that its expression is not a simple generalization of the formula from Bloch bands to BdG bands. We further verify the semiclassical result with a linear response approach. We implement the formula to study a toy model with a chiral p -wave pairing, and find that the chiral pairing alone is unable to produce nonzero orbital magnetic moment, which is in sharp contrast to the Berry curvatures [41, 44]. We show that the orbital magnetic moment can modulate the energy spectrum and the local density of states. Also, it can induce an orbital Nernst effect in superconductors. We study a honeycomb lattice with chiral d -wave pairing, and calculate the momentum-space distribution of orbital magnetic moment and the induced spectroscopic and transport responses.

* wangzh356@mail.sysu.edu.cn

The paper is organized as follows. In Sec. II, we derive the expression for the orbital magnetic moment of the superconducting quasiparticle in the semiclassical framework. In Sec. III, we verify the semiclassical result with a linear response approach. In Sec. IV, we compare the orbital magnetic moment with the orbital angular momentum. In Sec. V, we calculate the physical responses induced by the orbital magnetic moment. In Sec. VI, we present numerical studies of a tight-binding model with chiral d -wave superconducting gap.

II. SEMICLASSICAL THEORY FOR ORBITAL MAGNETIC MOMENT IN SUPERCONDUCTORS

The semiclassical theory for superconducting quasiparticles mathematically resembles the theory for Bloch electrons [41, 44], where the dynamics of the quasiparticle wavepacket is dominated by a local approximation of the Hamiltonian in which the position dependence of the external perturbation fields is approximated by the center position of the wavepacket \mathbf{r}_c . For the BdG Hamiltonian, the local approximation writes as,

$$\hat{H}_c = \begin{pmatrix} \hat{h}_0[\mathbf{r}_c, \mathbf{r}, \mathbf{p} + e\mathbf{A}(\mathbf{r}_c)] & \hat{\Delta}(\mathbf{r}_c, \mathbf{p}) \\ \hat{\Delta}(\mathbf{r}_c, \mathbf{p}) & -\hat{h}_0^*[\mathbf{r}_c, \mathbf{r}, \mathbf{p} + e\mathbf{A}(\mathbf{r}_c)] \end{pmatrix}, \quad (1)$$

where \hat{h}_0 is the electron Hamiltonian, $\mathbf{p} = -i\hbar\nabla_{\mathbf{r}}$ is the electron momentum operator and $-e$ is the electron charge, $\hat{\Delta}$ is the superconducting pairing Hamiltonian, and \mathbf{A} is the vector potential which was taken as the external perturbation field for the sake of studying orbital magnetic moment [10]. The momentum dependence of the pairing Hamiltonian reflects the pairing symmetry of the Cooper pair that involves the relative position of the two electrons of a Cooper pair [44], therefore it does not depend on the vector potential. This local Hamiltonian has the same spatial periodicity as the homogeneous bulk Hamiltonian, therefore it satisfies the eigenvalue equation

$$\hat{H}_c |\psi_{n,\mathbf{k},\mathbf{r}_c}\rangle = E_c |\psi_{n,\mathbf{k},\mathbf{r}_c}\rangle, \quad (2)$$

where E_c is the eigenenergy, $|\psi_{n,\mathbf{k},\mathbf{r}_c}\rangle = e^{i\mathbf{k}\cdot\mathbf{r}} |\phi_{n,\mathbf{k},\mathbf{r}_c}\rangle$ is the eigen function with $|\phi_{n,\mathbf{k},\mathbf{r}_c}\rangle$ being the cell-periodic part, n labels the BdG band and \mathbf{k} denotes the momentum. We can construct a quasiparticle wavepacket [11, 40, 44] at the n -th BdG band with these eigen functions

$$|\Psi_{\mathbf{k}_c, \mathbf{r}_c}\rangle = \int d\mathbf{k} \alpha_{\mathbf{k}} |\psi_{n,\mathbf{k},\mathbf{r}_c}\rangle, \quad (3)$$

where $\alpha_{\mathbf{k}} = |\alpha_{\mathbf{k}}| e^{-i\gamma_{\mathbf{k}}}$ is the constructing function, and $\mathbf{k}_c = \int d\mathbf{k} |\alpha_{\mathbf{k}}|^2 \mathbf{k}$ is the center of the wavepacket in the momentum space. The energy of the wavepacket E , evaluated up to the first order in the perturbation gradients, is given by:

$$E \approx \langle \Psi | \hat{H}_c | \Psi \rangle + \langle \Psi | \Delta \hat{H} | \Psi \rangle = E_c + \Delta E_{n,\mathbf{k}_c}, \quad (4)$$

where $\Delta E_{n,\mathbf{k}_c}$ is the wavepacket averaging over the gradient correction to the local Hamiltonian which writes as [11]

$$\Delta \hat{H} = \frac{1}{2} \left[(\hat{\mathbf{r}} - \mathbf{r}_c) \cdot \frac{\partial \hat{H}_c}{\partial \mathbf{r}_c} + \frac{\partial \hat{H}_c}{\partial \mathbf{r}_c} \cdot (\hat{\mathbf{r}} - \mathbf{r}_c) \right], \quad (5)$$

where $\hat{\mathbf{r}} = \mathbf{r}\tau_0$ is the quasiparticle position operator with τ_0 the identity matrix acting on the particle-hole space of the BdG Hamiltonian. In semiclassical theory, the orbital magnetic moment resides in the first-order energy corrections to the magnetic field. Therefore, we consider a homogeneous magnetic field \mathbf{B} with a circular gauge $\mathbf{A}(\mathbf{r}_c) = (\mathbf{B} \times \mathbf{r}_c)/2$. Then the gradient expansion of the local Hamiltonian writes as,

$$\Delta \hat{H} = \frac{e}{4m} \mathbf{B} \cdot [(\hat{\mathbf{r}} - \mathbf{r}_c) \times \mathbf{p}\tau_0 - \mathbf{p}\tau_0 \times (\hat{\mathbf{r}} - \mathbf{r}_c)], \quad (6)$$

where m is the mass of the electron. Then the first-order energy correction from a small homogeneous magnetic field is written as $\Delta E_{n,\mathbf{k}_c} = -\mathbf{B} \cdot \mathbf{m}_n(\mathbf{k}_c)$ where the orbital magnetic moment is given by

$$\mathbf{m}_n(\mathbf{k}_c) = -\frac{e}{4m} \langle \Psi | (\hat{\mathbf{r}} - \mathbf{r}_c) \times \hat{\mathbf{p}} | \Psi \rangle + \text{h.c.}, \quad (7)$$

where $\hat{\mathbf{p}} = \mathbf{p}\tau_0$ is the electron momentum operator acting on the particle-hole space.

The detailed calculation of this orbital magnetic moment resembles the one for the electron system [10]. A straightforward integration over the wavepacket function gives,

$$\mathbf{m}_n(\mathbf{k}_c) = -\frac{e}{2m} \text{Re} \left[\langle D_{\mathbf{k}} \phi_{n,\mathbf{k}} | \times \hat{\mathbf{p}}_{\mathbf{k}} | \phi_{n,\mathbf{k}} \rangle \right] |_{\mathbf{k}=\mathbf{k}_c}, \quad (8)$$

where $D_{\mathbf{k}} \equiv i\partial_{\mathbf{k}} - \mathbf{A}_{\mathbf{k}}$ is the gauge invariant \mathbf{k} -space derivative [44] with $\mathbf{A}_{\mathbf{k}} = i\langle \phi_{n,\mathbf{k}} | \partial_{\mathbf{k}} \phi_{n,\mathbf{k}} \rangle$ being the quasiparticle Berry connection, and $\hat{\mathbf{p}}_{\mathbf{k}} = e^{-i\mathbf{k}\cdot\mathbf{r}} \hat{\mathbf{p}} e^{i\mathbf{k}\cdot\mathbf{r}}$ is the \mathbf{k} -dependent momentum operator. From this formula we see that the orbital magnetic moment of each wavepacket depends only on its momentum-space center \mathbf{k}_c . Therefore, for simplicity, we omit the label c in the momentum \mathbf{k}_c below.

Now we try to explicitly evaluate the quantum averaging over the \mathbf{k} -dependent momentum operator $\hat{\mathbf{p}}_{\mathbf{k}}$ in Eq. (8). For this purpose, we use the relation $\hat{\mathbf{p}}_{\mathbf{k}} = (m/\hbar)\tau_z \partial_{\mathbf{k}} \hat{H}_{\mathbf{k}}^d$, where $\hat{H}_{\mathbf{k}}^d = \text{diag}(e^{-i\mathbf{k}\cdot\mathbf{r}} \hat{h}_0 e^{i\mathbf{k}\cdot\mathbf{r}}, -e^{-i\mathbf{k}\cdot\mathbf{r}} \hat{h}_0^* e^{i\mathbf{k}\cdot\mathbf{r}})$ depends only on the diagonal blocks of the BdG Hamiltonian, and τ_z is the Pauli matrix acting on the particle-hole space. We plug this expression into Eq. (8) and insert the identity operator $\sum_{n'} |\phi_{n',\mathbf{k}}\rangle \langle \phi_{n',\mathbf{k}}|$, and then the orbital magnetic moment can be written as

$$\mathbf{m}_n(\mathbf{k}) = \frac{e}{2\hbar} \sum_{n' \neq n} \text{Im} \left[\frac{\langle \phi_n | \partial_{\mathbf{k}} \hat{H}_{\mathbf{k}} | \phi_{n'} \rangle \times \langle \phi_{n'} | \tau_z \partial_{\mathbf{k}} \hat{H}_{\mathbf{k}}^d | \phi_n \rangle}{E_{n',\mathbf{k}} - E_{n,\mathbf{k}}} \right], \quad (9)$$

where $\hat{H}_{\mathbf{k}} = e^{-i\mathbf{k}\cdot\mathbf{r}} \hat{H}_c e^{i\mathbf{k}\cdot\mathbf{r}}$ is the \mathbf{k} -dependent Hamiltonian which satisfies the eigenvalue equation $\hat{H}_{\mathbf{k}} |\phi_{n,\mathbf{k}}\rangle = E_{n,\mathbf{k}} |\phi_{n,\mathbf{k}}\rangle$.

The expression (9) is the central result of this work. It is obviously gauge-invariant because the phase factors of eigen functions from the gauge transformation will cancel out. Comparing with the expression for Bloch electrons, there are two differences. Firstly, there is an extra τ_z factor that is coming from the effective charge of the BdG quasiparticle. Secondly, the formula involves not only the \mathbf{k} -dependent BdG Hamiltonian $H_{\mathbf{k}}$, but also its diagonal blocks $\hat{H}_{\mathbf{k}}^d$. This is due to the fact

that the vector gauge does not enter the effective momentum of the pairing gap. As a result, the quasiparticle orbital magnetic moment cannot come solely from the \mathbf{k} -dependence of the gap function, which is entirely different from the behavior of the quasiparticle Berry curvatures [41, 44].

For conventional s -wave superconductors where the pairing gap has no \mathbf{k} -dependence, we would have $\partial_{\mathbf{k}}\hat{H}_{\mathbf{k}} = \partial_{\mathbf{k}}\hat{H}_{\mathbf{k}}^d$. Then the quasiparticle orbital magnetic moment can be further expressed as derivatives to eigen functions,

$$\mathbf{m}_n(\mathbf{k}) = \frac{e}{2\hbar} \text{Re} \left[\langle D_{\mathbf{k}}\phi_{n,\mathbf{k}} | \times \tau_z (H_{\mathbf{k}} - E_{n,\mathbf{k}}) | \partial_{\mathbf{k}}\phi_{n,\mathbf{k}} \rangle \right] \quad (10)$$

$$- \frac{1}{2\hbar} \mathbf{d}_e \times \partial_{\mathbf{k}} E_{n,\mathbf{k}},$$

with $\rho_{\mathbf{k}} = e \langle \phi_{n,\mathbf{k}} | \tau_z | \phi_{n,\mathbf{k}} \rangle$ the effective charge of the wavepacket and $\mathbf{d}_e = e \text{Re} [\langle \phi_{n,\mathbf{k}} | \tau_z | i \partial_{\mathbf{k}} \phi_{n,\mathbf{k}} \rangle - \rho_{\mathbf{k}} \mathbf{A}_{\mathbf{k}} / e]$ the charge dipole of the wavepacket [44]. The first term resembles the orbital magnetic moment of the electrons, but with an extra τ_z matrix in the quantum averaging. This originates from the effective charge of the wavepacket which is exactly the quantum averaging over a τ_z matrix. The second term is the dipole induced current which comes from the fact that the charge center of the wavepacket is different from the probability center of the wavepacket.

III. LINEAR RESPONSE THEORY FOR ORBITAL MAGNETIC MOMENT IN SUPERCONDUCTORS

We can verify the semiclassical result with a linear response approach that was developed in Ref. [7] for studying the orbital magnetic moment of Bloch electrons. In this approach, the orbital magnetization can be obtained by the linear response of the grand thermodynamic potential at low temperature $K = E - \mu N$ with respect to the magnetic field. To get around the difficulty of the non-locality of the orbital magnetization operator, the magnetic field is introduced into the system with an infinitely slow spatial variation of

$$\mathbf{B}(\mathbf{r}) = \frac{B}{2} (\cos q_x x + \cos q_y y) \hat{\mathbf{z}}, \quad (11)$$

where B is the amplitude of the magnetic field, q_x and q_y are the wave vectors of the magnetic field along the two spatial directions. By adopting a convenient gauge, we can write

down the corresponding vector potential as

$$\mathbf{A}(\mathbf{r}) = \frac{B}{2} \left(\frac{\sin q_x x}{q_x} \hat{\mathbf{y}} - \frac{\sin q_y y}{q_y} \hat{\mathbf{x}} \right). \quad (12)$$

We will calculate the linear response to this gauge field and then take the long-wavelength limit that $q_{x,y}$ goes to zero to obtain the orbital magnetic moment that couples with the static magnetic field. We note that in this long-wavelength limit our gauge choice corresponds to the conventional circular gauge which is the same gauge we took in semiclassical calculations. Now the BdG Hamiltonian is written as

$$\hat{H}_{\text{BdG}} = \begin{pmatrix} \hat{h}_0[\mathbf{r}, \mathbf{p} + e\mathbf{A}] & \hat{\Delta}(\mathbf{p}) \\ \hat{\Delta}(\mathbf{p}) & -\hat{h}_0^*[\mathbf{r}, \mathbf{p} + e\mathbf{A}] \end{pmatrix}, \quad (13)$$

where the vector potential \mathbf{A} is given in Eq. (12). Now we can expand this BdG Hamiltonian to the linear order of the magnetic field $\hat{H}_{\text{BdG}} = \hat{H} + \Delta\hat{H}$ where $\hat{H} = \hat{H}_{\text{BdG}}(\mathbf{B} = 0)$ is the unperturbed BdG Hamiltonian with the quasiparticle band dispersion $E_{n,\mathbf{k}}$ and quasiparticle eigenstates $\psi_{n,\mathbf{k}}(\mathbf{r}) = e^{i\mathbf{k}\cdot\mathbf{r}} \phi_{n,\mathbf{k}}(\mathbf{r})$, and $\Delta\hat{H}$ is the first-order perturbation Hamiltonian induced by the magnetic field that is written as

$$\Delta\hat{H} = \frac{e}{2m} [\mathbf{p} \cdot \mathbf{A} + \mathbf{A} \cdot \mathbf{p}] \tau_0. \quad (14)$$

This perturbed Hamiltonian will induce a correction to the grand canonical ensemble energy density [7] $K(\mathbf{r}) = \sum_{n,\mathbf{k}} f_{n,\mathbf{k}} \text{Re} [\psi_{n,\mathbf{k}}^*(\mathbf{r}) \hat{H} \psi_{n,\mathbf{k}}(\mathbf{r})]$ with $f_{n,\mathbf{k}}$ being the occupation number of quasiparticles. Then the orbital magnetization can be obtained from the corresponding Fourier component $M_z = -\frac{2}{\sqrt{V}} \int d\mathbf{r} \delta K(\mathbf{r}) (\cos q_y y + \cos q_x x)$ where V is the system volume.

The first-order correction to the grand canonical ensemble energy density has contributions from the occupation number, the Hamiltonian, and the wave function:

$$\delta K(\mathbf{r}) = \text{Re} \sum_{n,\mathbf{k}} \left\{ \delta f_{n,\mathbf{k}} \psi_{n,\mathbf{k}}^* \hat{H} \psi_{n,\mathbf{k}} + f_{n,\mathbf{k}} \psi_{n,\mathbf{k}}^* \Delta\hat{H} \psi_{n,\mathbf{k}} + f_{n,\mathbf{k}} (\psi_{n,\mathbf{k}}^* \hat{H} \delta\psi_{n,\mathbf{k}} + \delta\psi_{n,\mathbf{k}}^* \hat{H} \psi_{n,\mathbf{k}}) \right\}. \quad (15)$$

The first two terms do not contribute to M_z after performing the spatial integration because of the cosine factors. The last two terms mainly involve the first-order corrections to the wave function which can be written by the standard first-order perturbation theory

$$\delta\psi_{n,\mathbf{k}}(\mathbf{r}) = \frac{eB}{8imq_x} \sum_{n'} \left[\frac{e^{i(\mathbf{k}+\mathbf{q}_x)\cdot\mathbf{r}} \langle \phi_{n',\mathbf{k}+\mathbf{q}_x} | \phi_{n,\mathbf{k}} \rangle \langle \phi_{n',\mathbf{k}+\mathbf{q}_x} | \hat{p}_{\mathbf{k}}^y + \hat{p}_{\mathbf{k}+\mathbf{q}_x}^y | \phi_{n,\mathbf{k}} \rangle}{E_{n,\mathbf{k}} - E_{n',\mathbf{k}+\mathbf{q}_x}} - (\mathbf{q}_x \rightarrow -\mathbf{q}_x) \right]$$

$$- \frac{eB}{8imq_y} \sum_{n'} \left[\frac{e^{i(\mathbf{k}+\mathbf{q}_y)\cdot\mathbf{r}} \langle \phi_{n',\mathbf{k}+\mathbf{q}_y} | \phi_{n,\mathbf{k}} \rangle \langle \phi_{n',\mathbf{k}+\mathbf{q}_y} | \hat{p}_{\mathbf{k}}^x + \hat{p}_{\mathbf{k}+\mathbf{q}_y}^x | \phi_{n,\mathbf{k}} \rangle}{E_{n,\mathbf{k}} - E_{n',\mathbf{k}+\mathbf{q}_y}} - (\mathbf{q}_y \rightarrow -\mathbf{q}_y) \right], \quad (16)$$

where $\mathbf{q}_x = (q_x, 0, 0)$ and $\mathbf{q}_y = (0, q_y, 0)$. Substituting this

wave function correction $\delta\psi_{n,\mathbf{k}}$ into Eq. (15) and performing

the spatial integration of M_z , we can obtain the orbital magnetization \mathbf{M} by taking the long-wavelength limit of $\mathbf{q} \rightarrow 0$ and generalizing the result to other components [7]. In the expression of the orbital magnetization, we find that significant contributions come from the orbital magnetic moment of the quasiparticles which is written as

$$\mathbf{m}_n(\mathbf{k}) = \frac{e}{2\hbar} \sum_{n' \neq n} \text{Im} \left[\frac{\langle \phi_n | \partial_{\mathbf{k}} \hat{H}_{\mathbf{k}} | \phi_{n'} \rangle \times \langle \phi_{n'} | \tau_z \partial_{\mathbf{k}} \hat{H}_{\mathbf{k}}^d | \phi_n \rangle}{E_{n',\mathbf{k}} - E_{n,\mathbf{k}}} \right]. \quad (17)$$

Here we use the relation $\hat{\mathbf{p}}_{\mathbf{k}} = (m/\hbar)\tau_z \partial_{\mathbf{k}} \hat{H}_{\mathbf{k}}^d$ again. It is clear that this result is identical to that in Eq. (9). This linear response approach for calculating the orbital magnetic moment verifies our semiclassical results.

IV. ORBITAL MAGNETIC MOMENT AND ORBITAL ANGULAR MOMENTUM IN SUPERCONDUCTORS

The effective charge of Bogoliubov quasiparticles is not a conserved quantity, because Bogoliubov quasiparticles are quantum superposition of electrons and holes where the superposition ratio may vary during dynamical processes. In the wavepacket approach, this is reflected in the fact that the charge center of the quasiparticle wavepacket generally does not coincide with its probability center. Consequently, the expression for the orbital magnetic moment is quite unique for superconductors. We can see this more clearly by comparing the quasiparticle's orbital magnetic moment with its orbital angular momentum.

The orbital angular momentum of a Bogoliubov quasiparticle can be obtained by the wavepacket averaging over the angular momentum operator $\hat{\mathbf{L}} = \hat{\mathbf{r}} \times \hat{\mathbf{P}}$ where $\hat{\mathbf{r}}$ and $\hat{\mathbf{P}}$ are the quasiparticle position and momentum operators. Following a similar derivation of Eq. (9) and taking the relation of $\hat{\mathbf{P}}_{\mathbf{k}} = (m/\hbar)\partial_{\mathbf{k}} \hat{H}_{\mathbf{k}}$ for the quasiparticle momentum operator, we obtain the angular momentum of a wavepacket as

$$\mathbf{L}_n(\mathbf{k}) = -\frac{m}{\hbar} \sum_{n' \neq n} \text{Im} \left[\frac{\langle \phi_n | \partial_{\mathbf{k}} \hat{H}_{\mathbf{k}} | \phi_{n'} \rangle \times \langle \phi_{n'} | \partial_{\mathbf{k}} \hat{H}_{\mathbf{k}} | \phi_n \rangle}{E_{n',\mathbf{k}} - E_{n,\mathbf{k}}} \right]. \quad (18)$$

This expression for the orbital angular momentum formally resembles the one for electron systems and looks similar to the expression of the quasiparticle Berry curvature with the only difference in the denominator: the orbital angular momentum is the energy difference of two BdG bands while the Berry curvature is the square of the energy difference [41, 44]. Comparing Eq. (18) and Eq. (9), we can see that the difference between the orbital angular momentum and the orbital magnetic moment is the replacement of $\partial_{\mathbf{k}} \hat{H}_{\mathbf{k}}$ with $\tau_z \partial_{\mathbf{k}} \hat{H}_{\mathbf{k}}^d$ in the numerator. This difference is due to the fact that the self-rotation of the charge distribution is different from the self-rotation of the probability distribution within a wavepacket, which is a unique feature of the charge non-conserved Bogoliubov quasiparticles. The τ_z matrix in the expression of the magnetic moment comes from the superposition of the electron and hole components which have opposite charges, while the derivative

over the diagonal component of the BdG Hamiltonian reflects the fact that the energy gap describes the relative wave function of the Cooper pair which does not directly couple with the gauge field.

The fact that the relative wave function of the energy gap does not directly couple with the orbital magnetic moment has qualitative impacts. As a result, a chiral superconductivity does not necessarily have nonzero orbital magnetic moment even though the orbital angular momentum is nonzero. To see this point clearly, we consider the simplest chiral p -wave superconductor which can be described by a 2×2 BdG Hamiltonian as,

$$\hat{H}_{\mathbf{k}} = \begin{pmatrix} \xi_{\mathbf{k}} & \Delta_0(k_x + ik_y) \\ \Delta_0(k_x - ik_y) & -\xi_{-\mathbf{k}} \end{pmatrix}, \quad (19)$$

where $\xi_{\mathbf{k}} = \hbar^2 k^2 / (2m) - \mu$ is the electron dispersion with μ the chemical potential and Δ_0 represents the energy gap amplitude. For this model, the orbital angular momentum and the orbital magnetic moment are exactly solvable. We find a finite orbital angular momentum of $L(\mathbf{k}) = m\Delta_0^2(\xi_{\mathbf{k}} + 2\mu)/(\hbar E_{\mathbf{k}}^2)$ with $E_{\mathbf{k}} = \sqrt{\xi_{\mathbf{k}}^2 + \Delta_0^2 k^2}$ the quasiparticle dispersion, while the orbital magnetic moment vanishes in the entire momentum space

$$m(\mathbf{k}) = 0. \quad (20)$$

The chiral p -wave gap induces nonzero Berry curvature $\Omega(\mathbf{k})$ and orbital angular momentum, and the two satisfy a relation $L(\mathbf{k}) = -2(m/\hbar)E_{\mathbf{k}}\Omega(\mathbf{k})$ similar to that for Bloch electrons [24]. In contrast, for orbital magnetic moment the derivative $\tau_z \partial_{\mathbf{k}} \hat{H}_{\mathbf{k}}^d$ gives an identity matrix, therefore we have $\langle \phi_{n'} | \tau_z \partial_{\mathbf{k}} \hat{H}_{\mathbf{k}}^d | \phi_n \rangle = \partial_{\mathbf{k}} \xi_{\mathbf{k}} \langle \phi_{n'} | \phi_n \rangle = 0$ since $n' \neq n$. This behavior is quite different from Bloch electrons, where a finite Berry curvature is generically accompanied by a finite orbital magnetic moment [10, 12, 24].

For a general two-band BdG Hamiltonian, a chiral superconducting gap can induce a nonzero orbital magnetic moment if the electron dispersion is not symmetric with respect to the momentum $\xi_{\mathbf{k}} \neq \xi_{-\mathbf{k}}$. Therefore, the diagonal part of the BdG Hamiltonian can be written as $\hat{H}_{\mathbf{k}}^d = \xi_{\mathbf{k}}^a \tau_0 + \xi_{\mathbf{k}}^b \tau_z$, where $\xi_{\mathbf{k}}^a = (\xi_{\mathbf{k}} - \xi_{-\mathbf{k}})/2$ and $\xi_{\mathbf{k}}^b = (\xi_{\mathbf{k}} + \xi_{-\mathbf{k}})/2$. Then the quantum averaging writes as $\langle \phi_{n'} | \tau_z \partial_{\mathbf{k}} \hat{H}_{\mathbf{k}}^d | \phi_n \rangle = \partial_{\mathbf{k}} \xi_{\mathbf{k}}^a \langle \phi_{n'} | \tau_z | \phi_n \rangle$, where we take the orthogonality relation between the eigen function of different BdG bands. The nonzero $\xi_{\mathbf{k}}^a$ can be achieved by breaking the spatial inversion symmetry or the time-reversal symmetry in the electron Hamiltonian, or by driving a supercurrent that produces a Doppler shift of the BdG spectrum [44, 53, 54]. In multiband systems, additional internal structure in the electron Hamiltonian can make $\tau_z \partial_{\mathbf{k}} \hat{H}_{\mathbf{k}}^d$ not proportional to the identity operator, thereby yielding a nonzero matrix element $\langle \phi_{n'} | \tau_z \partial_{\mathbf{k}} \hat{H}_{\mathbf{k}}^d | \phi_n \rangle$, as exemplified by the honeycomb lattice model discussed in Sec. VI.

V. RESPONSES INDUCED BY ORBITAL MAGNETIC MOMENTS

The orbital magnetic moment of Bogoliubov quasiparticles widely influences the spectroscopic and transport properties of superconducting systems. First of all, by definition the orbital magnetic moment modifies the energy spectrum with a term that is linear in the applied magnetic field. This energy correction induces a first-order energy shift for the Bogoliubov band at momentum \mathbf{k} ,

$$\Delta E_{n,\mathbf{k}} = -\mathbf{B} \cdot \mathbf{m}_n(\mathbf{k}). \quad (21)$$

This energy shift for the quasiparticles can be observed directly by spectroscopic methods such as angle-resolved photoemission spectroscopy [55]. This should be a small energy shift because the magnetic field applied to superconductors usually cannot be too large. However, it may be large enough for experimental detection in the momentum areas where the orbital magnetic moment concentrates. Secondly, accompanying the shift of the quasiparticle energy spectrum, one expects a corresponding modification in the density of states. For superconductors, the field-corrected density of states is given by

$$n(E) = \sum_n \int d\mathbf{k} [|u|^2 \delta(E - E_{n,\mathbf{k}}^m) + |v|^2 \delta(E + E_{n,\mathbf{k}}^m)], \quad (22)$$

where $E_{n,\mathbf{k}}^m = E_{n,\mathbf{k}} - \mathbf{B} \cdot \mathbf{m}_n(\mathbf{k})$ is the quasiparticle band dispersion corrected by the orbital magnetic moment, u and v are the electron and hole components of the BdG eigen function. We compare the field-corrected density of states $n(E)$ with the zero-field counterpart $n_0(E) = n(\mathbf{B} = 0)$, and define their difference as $\delta n(E) = n(E) - n_0(E)$. Due to the orbital magnetic moment, the presence of an external magnetic field leads to a nonzero correction in the density of states. Because $\mathbf{m}_n(\mathbf{k})$ is \mathbf{k} -dependent, energy shifts $\Delta E_{n,\mathbf{k}}$ are generically nonuniform across the Brillouin zone and give rise to energy-dependent enhancement and suppression in the local density of states, which can be measured directly via scanning tunneling spectroscopy [56].

Aside from the influence on the spectroscopic properties, the quasiparticle orbital magnetic moment can also give rise to orbital Hall transport in superconductors. Here we examine the orbital Nernst response where a temperature gradient is applied to the superconductor as a driving force for the quasiparticles. In the semiclassical picture, each wavepacket carries an orbital magnetic moment $\mathbf{m}_{\mathbf{k}_c}$ and moves with the velocity $\dot{\mathbf{r}}_c$ [44]. Combining together, a wavepacket contributes an orbital magnetic moment current of $\mathbf{j}^\alpha = m_{\mathbf{k}_c}^\alpha \dot{\mathbf{r}}_c$ where $\alpha = \{x, y, z\}$ denotes components of the orbital magnetic moment. Summing over wavepackets gives the total orbital magnetic moment current density

$$\mathbf{J}^\alpha(\mathbf{r}) = \sum_n \int d\mathbf{k}_c f_{\mathbf{k}_c} m_{\mathbf{k}_c}^\alpha \dot{\mathbf{r}}_c |_{\mathbf{r}_c=\mathbf{r}}. \quad (23)$$

The wavepacket velocity is determined by the equation of motions which has been derived for superconductors [41, 44]. For

linear intrinsic Hall response, we can simplify the equation of motion as $\dot{\mathbf{r}}_c = -\dot{\mathbf{k}}_c \times \boldsymbol{\Omega}_{\mathbf{k}_c} = (\nabla_{\mathbf{r}_c} E / \hbar) \times \boldsymbol{\Omega}_{\mathbf{k}_c}$ and then the orbital magnetic moment current density writes as,

$$\mathbf{J}^\alpha(\mathbf{r}) = \sum_n \frac{1}{\hbar} \int d\mathbf{k}_c f_{\mathbf{k}_c} m_{\mathbf{k}_c}^\alpha [\nabla_{\mathbf{r}_c} E \times \boldsymbol{\Omega}_{\mathbf{k}_c}]_{\mathbf{r}_c=\mathbf{r}}, \quad (24)$$

where $f_{\mathbf{k}_c}$ reduces to the Fermi distribution function because we take the zeroth-order approximation for the occupation number of the quasiparticles. Now we take care of the spatial gradient to the energy $\nabla_{\mathbf{r}_c} E$ in the presence of a temperature gradient by introducing the quasiparticle grand potential function $g(E, T) = k_B T \ln(1 - f)$ with k_B the Boltzmann constant and T the temperature. It satisfies the relation $f = \partial g / \partial E$ and the transport part of the orbital magnetic moment current can be expressed as $\mathbf{J}^\alpha(\mathbf{r}) = \boldsymbol{\eta}^\alpha \times \nabla_{\mathbf{r}} T$ with the orbital Nernst coefficient given by

$$\boldsymbol{\eta}^\alpha = \sum_n \frac{1}{\hbar} \int d\mathbf{k}_c \frac{\partial g}{\partial T} m_{\mathbf{k}_c}^\alpha \boldsymbol{\Omega}_{\mathbf{k}_c}. \quad (25)$$

This formula resembles the one for the spin Nernst coefficient of the superconductors only with the effective spin of each wavepacket replaced by the orbital magnetic moment [44, 49]. It requires the simultaneous existence of the orbital magnetic moment and the Berry curvature of Bogoliubov quasiparticles, which places a stricter constraint on the structure of the BdG Hamiltonian.

VI. MODEL CALCULATIONS

We have demonstrated that generating a quasiparticle orbital magnetic moment requires a suitable combination of electronic band structure and superconducting pairing function. Here we consider a two-dimensional tight-binding model with a honeycomb lattice that was introduced in Ref. [57]. This model inherently possesses the sub-lattice degrees of freedom, which, combined with a chiral pairing gap, fulfills the symmetry and structural requirements for generating a finite orbital magnetic moment. The system consists of two sub-lattices with the Hamiltonian given by

$$\begin{aligned} \hat{H} = & -t \sum_{i,\beta,\sigma} [c_{A,i,\sigma}^\dagger c_{B,i+\delta_\beta,\sigma} + \text{h.c.}] \\ & - \mu \sum_{i,\sigma} (c_{A,i,\sigma}^\dagger c_{A,i,\sigma} + c_{B,i+\delta_1,\sigma}^\dagger c_{B,i+\delta_1,\sigma}) \\ & + \sum_{i,\beta} [\Delta_{\delta_\beta} (c_{A,i,\uparrow}^\dagger c_{B,i+\delta_\beta,\downarrow}^\dagger - c_{A,i,\downarrow}^\dagger c_{B,i+\delta_\beta,\uparrow}^\dagger) + \text{h.c.}], \end{aligned} \quad (26)$$

where A and B denote the two sub-lattices of a unit cell, $\sigma = \uparrow, \downarrow$ denotes the spin index, i denotes the A sub-lattice site with position \mathbf{r}_i , δ_β with $\beta = \{1, 2, 3\}$ denotes the three vectors that connect the nearest A and B sub-lattices which are given as $\delta_1 = (a, -\sqrt{3}a)/(2\sqrt{3})$, $\delta_2 = (a, \sqrt{3}a)/(2\sqrt{3})$ and $\delta_3 = (-a, 0)/\sqrt{3}$ with a the lattice constant, c_A^\dagger and c_B^\dagger are the creation operators on the A and B sub-lattices respectively, $\Delta_{\delta_\beta} = \Delta e^{2i\beta\pi/3}$ represents the chiral d -wave pairing in the

honeycomb lattice with Δ the pairing amplitude, and t is the nearest-neighbor hopping amplitude.

This Hamiltonian can be transformed to the momentum space through the Fourier transformation of $c_{A,\mathbf{k},\sigma}^\dagger = (1/\sqrt{N}) \sum_i e^{i\mathbf{k}\cdot\mathbf{r}_i} c_{A,i,\sigma}^\dagger$ and $c_{B,\mathbf{k},\sigma}^\dagger = (1/\sqrt{N}) \sum_i e^{i\mathbf{k}\cdot(\mathbf{r}_i+\delta_\beta)} c_{B,i+\delta_\beta,\sigma}^\dagger$, where N is the number of sites of each sub-lattice. By defining a Nambu spinor of $\Psi_{\mathbf{k}} = (c_{A,\mathbf{k},\uparrow}, c_{B,\mathbf{k},\uparrow}, c_{A,-\mathbf{k},\downarrow}^\dagger, c_{B,-\mathbf{k},\downarrow}^\dagger)^T$, the Hamiltonian can be compactly written as $\hat{H} = \sum_{\mathbf{k}} \Psi_{\mathbf{k}}^\dagger \hat{H}_{\mathbf{k}} \Psi_{\mathbf{k}}$ where we obtain a 4×4 BdG matrix

$$\hat{H}_{\mathbf{k}} = \begin{pmatrix} -\mu & \tilde{f}_{\mathbf{k}} & 0 & \Delta_{\mathbf{k}} \\ \tilde{f}_{\mathbf{k}}^* & -\mu & \Delta_{-\mathbf{k}} & 0 \\ 0 & \Delta_{-\mathbf{k}}^* & \mu & -\tilde{f}_{-\mathbf{k}}^* \\ \Delta_{\mathbf{k}}^* & 0 & -\tilde{f}_{-\mathbf{k}} & \mu \end{pmatrix}, \quad (27)$$

with $\tilde{f}_{\mathbf{k}} = -t \sum_{\beta=1}^3 e^{i\mathbf{k}\cdot\delta_\beta}$ and $\Delta_{\mathbf{k}} = \sum_{\beta=1}^3 \Delta_{\delta_\beta} e^{i\mathbf{k}\cdot\delta_\beta}$. This Hamiltonian provides a simple example for the numerical calculation of the orbital magnetic moments.

A. Orbital magnetic moment distribution in momentum space

The electron band structure of the honeycomb-lattice system has Dirac cones at the K points of the Brillouin zone as shown in Fig. 1(b). In order for a robust superconducting gap, a finite area of electron Fermi surface is required. For this purpose, we consider the system to be tuned to deviate slightly from charge neutrality with the chemical potential shown as the dashed line in Fig. 1(b). In this case, the electron Fermi surface is shaped as six small pockets around the six Dirac points. The quasiparticle Berry curvature of this model has been calculated [41, 44]. As shown in Fig. 1(a), the quasiparticle Berry curvature is induced by the chiral d -wave pairing and concentrates on the electron Fermi surfaces.

Now we calculate the distribution of orbital magnetic moments in the momentum space for this model. In Fig. 1(c), we show the orbital magnetic moment $m^z(\mathbf{k})$ computed for the lowest positive-energy band under the same parameters as in Fig. 1(a). Although the orbital magnetic moment is also predominantly concentrated near the K points similar to the behavior of Berry curvatures, a clear distinction emerges between the fine structures of their distributions. This can be clearly seen from the insets of Figs. 1(a) and 1(c). The Berry curvature is peaked at the F points where the electronic Fermi surface resides, while the orbital magnetic moment peaks exactly at the K point. This is quite different from Bloch electrons where the peaks of the orbital magnetic moment and Berry curvatures often coincide with each other [24].

To understand this contrasting behavior, we analyze the BdG band structure shown in Fig. 1(d). Both the orbital magnetic moment and the Berry curvature depend on the energy differences between BdG bands. Specifically, the orbital magnetic moment scales as $1/(E_{n',\mathbf{k}} - E_{n,\mathbf{k}})$, whereas the Berry curvature scales as $1/(E_{n',\mathbf{k}} - E_{n,\mathbf{k}})^2$ [41, 44]. Thus, small energy gaps may enhance both quantities. Focusing on the band $n = 2$ shown in Fig. 1(d), we observe that the global minimum of the energy difference with $n' = 3$ happens at F points.

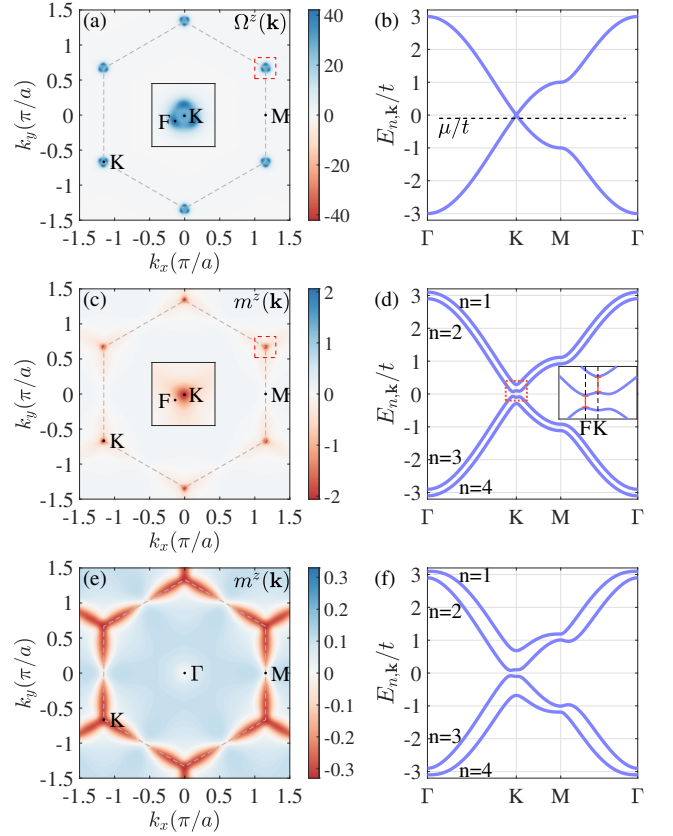


FIG. 1. (a) Momentum-space distribution of the Berry curvature $\Omega^z(\mathbf{k})$ (in units of a^2) for the lowest positive-energy band $n = 2$. The gray dashed lines denote the boundary of the first Brillouin zone. The high-symmetry points are marked with black dots. The inset is the zoom-in view of the red-dashed region. The parameters are taken as $\mu/t = -0.1$ and $\Delta/t=0.09$. (b) Electronic band structure along the high-symmetry lines. The dashed line indicates the chemical potential with $\mu/t = -0.1$. (c) Momentum-space distribution of the orbital magnetic moment $m^z(\mathbf{k})$ (in units of $a^2 et/\hbar$) for the lowest positive-energy band $n = 2$, with the parameters taken the same as in panel (a). (d) Quasiparticle band structure along the high-symmetry lines with parameters taken the same as in panel (a). (e) and (f) The momentum-space distribution of the orbital magnetic moment and the quasiparticle band structure along the high-symmetry lines with a different parameter of $\Delta/t=0.225$. The chemical potential is taken the same as in panel (a).

This small band gap is responsible for the large quasiparticle Berry curvatures as shown in Fig. 1(a). However, the orbital magnetic moment is suppressed, because the matrix element $\langle \phi_{n',\mathbf{k}} | \tau_z \partial_{\mathbf{k}} \hat{H}_{\mathbf{k}}^d | \phi_{n,\mathbf{k}} \rangle$ for bands $n = 2$ and $n' = 3$ vanishes at the F points. The other local minimum of the energy difference happens at K points between the two bands $n = 2$ and $n' = 1$. This local band gap minimum is responsible for the enlargement of the orbital magnetic moment since the matrix elements $\langle \phi_{n',\mathbf{k}} | \tau_z \partial_{\mathbf{k}} \hat{H}_{\mathbf{k}}^d | \phi_{n,\mathbf{k}} \rangle$ for bands $n = 2$ and $n' = 1$ are nonzero.

In Fig. 1(e), we show the momentum-space distribution of the orbital magnetic moment for a larger superconducting gap. In this case, the orbital magnetic moment is no longer strongly

localized at the K points but becomes more extended across the Brillouin zone. The corresponding band structure, as shown in Fig. 1(f), reveals that the overall energy gaps between different bands are generally larger than those in Fig. 1(d), therefore, the amplitudes of the orbital magnetic moment are smaller than the latter.

B. Spectroscopic properties: energy correction and density of states correction

The distribution of the orbital magnetic moment in momentum space directly influences the momentum-space energy spectrum in the presence of a magnetic field, as shown in Eq. (21). Here we perform numerical calculations of this energy correction for the honeycomb lattice with a uniform magnetic field $\mathbf{B} = B_z \hat{z}$. We present the energy correction $\Delta E_{n,\mathbf{k}}$ for the two positive energy BdG bands in Fig. 2(a), while the corrections to the negative-energy BdG bands can be obtained through particle-hole symmetry. It is obvious that the shift of the energy spectrum by the magnetic field coincides with the distribution of the orbital magnetic moment. The significant energy shifts concentrate near the K points in the momentum space, predominantly reducing the quasiparticle energies, and the energy correction of band $n = 1$ is larger than those of band $n = 2$. As a result, the BdG gaps are reduced by the energy shift from the coupling of orbital magnetic moment with the external field.

The corrections to the energy spectrum will modulate the density of states as shown in Eq. (22). We present the zero-field density of states $n_0(E)$ and its correction $\delta n(E)$ in Fig. 2(b). The $\delta n(E)$ curves exhibit distinct peaks and dips, indicating energies where the orbital magnetic moment has the largest modifications to the density of states. Notably, the $\delta n(E)$ curve shows an equal number of peaks and dips in both $E > 0$ and $E < 0$ regions, occurring at symmetric energies. In Figs. 2(c) and 2(d), we present the BdG band structure and mark these characteristic energies. We find that the two peaks closest to $E = 0$ correspond to the energies at the F points of bands $n = 2$ and $n = 3$. As shown in Fig. 2(a), the orbital magnetic moment reduces the energies near the K points of the positive-energy bands, including those at the F points of the band $n = 2$. It also increases the energies at the F points of the band $n = 3$, effectively narrowing the superconducting gap. This increases the number of in-gap states and results in a positive density of states correction which generates the two peaks nearest to $E = 0$ in $\delta n(E)$. The two dips correspond to the energies at the K points of bands $n = 2$ and $n = 3$. The substantial orbital magnetic moment at these points induces significant energy shifts, therefore, both the energy decreases at the K points of the band $n = 2$ and the energy increases at the K points of the band $n = 3$ reduce the number of states and lead to the observed dips in $\delta n(E)$. The two peaks farthest from $E = 0$ originate from energy modifications at the K points of bands $n = 1$ and $n = 4$. The large orbital magnetic moments at these points cause the energy of band $n = 1$ to decrease and that of band $n = 4$ to increase. These shifts enhance the number of states within the corrected energy intervals, thereby forming

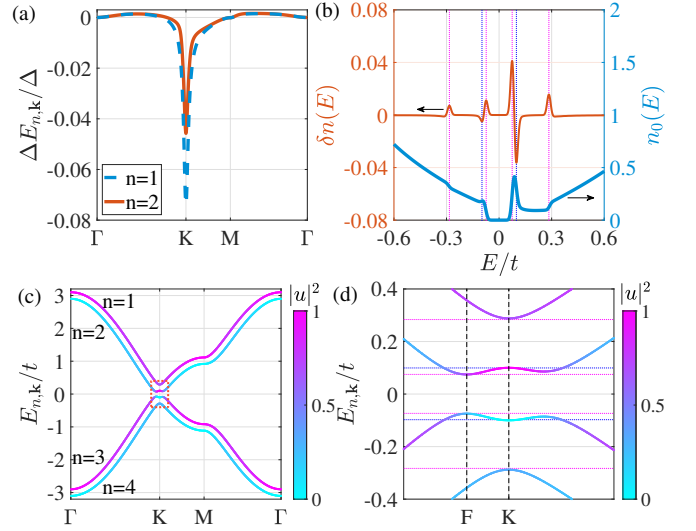


FIG. 2. (a) The ratio between energy correction $\Delta E_{n\mathbf{k}}$ due to a uniform magnetic field and pairing amplitude Δ for the positive-energy quasiparticle bands. (b) Field-induced density of states correction $\delta n(E)$ (orange line, left axis) and local density of states $n_0(E)$ in the absence of a magnetic field (blue line, right axis). The peaks and dips in $\delta n(E)$ are marked by pink dashed lines and blue dashed lines, respectively. (c) Quasiparticle band structure. The color scale represents the weight of the electron component $|u|^2$ with respect to the local density of states. (d) Zoom-in view of the red-dashed region in panel (c), showing the detailed band structure near the K point and F point. The horizontal dashed lines mark the characteristic energies corresponding to the peaks and dips in the density of states correction $\delta n(E)$ shown in panel (b), using the same color coding. The parameters used are $B_z = -(\hbar/a^2 e)/500$, $\Delta/t = 0.09$ and $\mu/t = -0.1$.

the peak structures in $\delta n(E)$.

Furthermore, we observe that the peaks and dips in $\delta n(E)$ have different magnitudes in the $E > 0$ and $E < 0$ regions, with a larger magnitude in the former region. This asymmetry can be understood by examining the contributions from the electron and the hole components of the quasiparticle wave functions. The local density of states is determined by both the quasiparticle energy $E_{n,\mathbf{k}}$ and the squared moduli of the electron and the hole wave functions, $|u|^2$ and $|v|^2$, as given in Eq. (22). We show the value of $|u|^2$ as the color map in Fig. 2(c) and Fig. 2(d), and the value of $|v|^2$ can be obtained by the normalization requirement $|v|^2 = 1 - |u|^2$. We find that around the F points the positive-energy $n = 2$ band has an overwhelming $|u|^2$ weight while the negative-energy $n = 3$ band has an overwhelming $|v|^2$ weight. As a result, the weight factors determining the density of states of the energy at the positive-energy peak are significantly larger than those at the corresponding negative-energy peak. Therefore, it is natural that the density of states correction is larger in the positive-energy region.

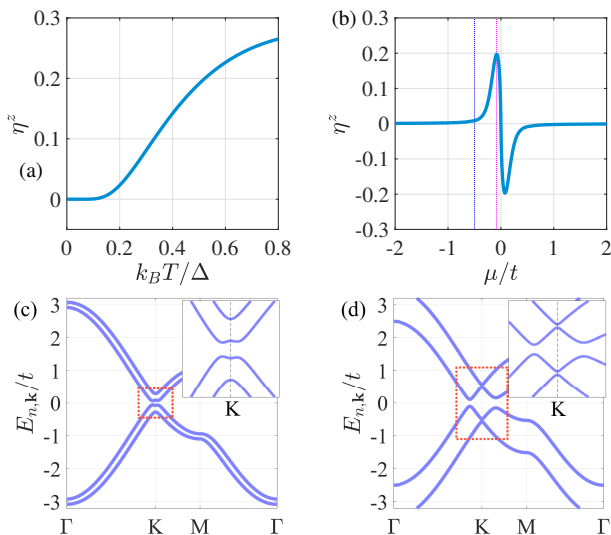


FIG. 3. (a) Temperature dependence of the orbital Nernst coefficient η^z (in units of $a^2 e t k_B / \hbar^2$) at fixed $\mu/t = -0.1$. (b) Chemical potential dependence of the orbital Nernst coefficient at fixed $k_B T / \Delta = 0.5$. (c) Quasiparticle band structure along the high-symmetry lines with $\mu/t = -0.015$. This chemical potential corresponds to the position marked by the pink dashed line in panel (b). The inset shows a detailed view near the K point. (d) Quasiparticle band structure with $\mu/t = -0.5$. This chemical potential corresponds to the position marked by the blue dashed line in panel (b). The other parameter used is $\Delta/t = 0.09$.

C. Transport property: orbital Nernst effect

The orbital magnetic moment not only strongly influences the spectroscopic properties of superconductors, but also induces the orbital Nernst effect in combination with non-trivial Berry curvatures as shown in Eq. (25). For the two-dimensional model Hamiltonian Eq. (27), the orbital Nernst coefficient η^α becomes a scalar η^α . We calculate η^z and show the temperature and chemical potential dependence in Fig. 3(a) and Fig. 3(b). The temperature dependence of the orbital Nernst coefficient η^z is quite simple: it increases monotonically with increasing temperature. This is due to the increase of the number of quasiparticles which is roughly determined by the factor of $1/(1 + e^{\Delta/k_B T})$. As for the chemical potential dependence, we find that η^z is exactly zero when the chemical potential locates at the Dirac point, which may simply be due to the vanishing electron density of states. When the chemical

potential deviates from the Dirac points, two peaks appear and then η^z gradually decreases.

To understand these transport features, we show the BdG band structure for two typical chemical potentials in Fig. 3(c) and Fig. 3(d), focusing on the K point where a substantial orbital magnetic moment emerges. The band structure shown in Fig. 3(c) corresponds to the chemical potential at the peak of the orbital Nernst coefficient marked by the pink dashed line in Fig. 3(b). It exhibits small band gaps at the K points which generate large orbital magnetic moments and consequently give rise to the significant orbital Nernst effect. As the chemical potential shifts away from the Dirac point to the position indicated by the blue dashed line in Fig. 3(b), the orbital Nernst coefficient diminishes. The corresponding band structure is shown in Fig. 3(d). We can see that while the band gaps at the K points remain small, the energies of the K points now deviate notably from zero, significantly suppressing the magnitude of the derivative $\partial g / \partial T$. Consequently, despite the persistent small band gap, the orbital Nernst coefficient becomes smaller.

VII. CONCLUSION

In summary, we have derived the orbital magnetic moment of superconducting quasiparticles with a semiclassical approach. By constructing a wavepacket with the Bogoliubov eigenstates, we calculate the energy of the wavepacket up to the linear order of the magnetic field and obtain the expression for the orbital magnetic moment. We verified the semiclassical result with a linear response approach. By comparing with the orbital angular momentum of the quasiparticle wavepacket, we reveal that the orbital magnetic moment has a more complicated structure. As a result, chiral superconductivity alone does not necessarily generate a nonzero orbital magnetic moment. We investigate the response of the superconducting quasiparticles due to the orbital magnetic moment, such as the magnetic modifications to the BdG band structure, corrections to the density of states, and the induced orbital Nernst effect. We apply our theoretical framework to a chiral d -wave superconductor on a honeycomb lattice. We show that the distribution of orbital magnetic moment can significantly deviate from the distribution of Berry curvatures, highlighting a fundamental departure from electronic systems. We calculate the responses and present their temperature and chemical potential dependence.

-
- [1] R. Resta, Electrical polarization and orbital magnetization: the modern theories, *Journal of Physics: Condensed Matter* **22**, 123201 (2010).
 [2] T. Thonhauser, Theory of orbital magnetization in solids, *International Journal of Modern Physics B* **25**, 1429 (2011).
 [3] F. Aryasetiawan and K. Karlsson, Modern theory of orbital magnetic moment in solids, *Journal of Physics and Chemistry of*

- Solids* **128**, 87 (2019), spin-Orbit Coupled Materials.
 [4] R. B. Atencia, A. Agarwal, and D. Culcer, Orbital angular momentum of Bloch electrons: equilibrium formulation, magneto-electric phenomena, and the orbital Hall effect, *Advances in Physics: X* **9**, 2371972 (2024).
 [5] T. Thonhauser, D. Ceresoli, D. Vanderbilt, and R. Resta, Orbital magnetization in periodic insulators, *Phys. Rev. Lett.* **95**, 137205

- (2005).
- [6] D. Ceresoli, T. Thonhauser, D. Vanderbilt, and R. Resta, Orbital magnetization in crystalline solids: Multi-band insulators, Chern insulators, and metals, *Phys. Rev. B* **74**, 024408 (2006).
- [7] J. Shi, G. Vignale, D. Xiao, and Q. Niu, Quantum theory of orbital magnetization and its generalization to interacting systems, *Phys. Rev. Lett.* **99**, 197202 (2007).
- [8] D. Xiao, J. Shi, and Q. Niu, Berry phase correction to electron density of states in solids, *Phys. Rev. Lett.* **95**, 137204 (2005).
- [9] D. Xiao, Y. Yao, Z. Fang, and Q. Niu, Berry-phase effect in anomalous thermoelectric transport, *Phys. Rev. Lett.* **97**, 026603 (2006).
- [10] M.-C. Chang and Q. Niu, Berry phase, hyperorbits, and the Hofstadter spectrum: Semiclassical dynamics in magnetic Bloch bands, *Phys. Rev. B* **53**, 7010 (1996).
- [11] G. Sundaram and Q. Niu, Wave-packet dynamics in slowly perturbed crystals: Gradient corrections and Berry-phase effects, *Phys. Rev. B* **59**, 14915 (1999).
- [12] D. Xiao, M.-C. Chang, and Q. Niu, Berry phase effects on electronic properties, *Rev. Mod. Phys.* **82**, 1959 (2010).
- [13] S. Lahiri, T. Bhore, K. Das, and A. Agarwal, Nonlinear magnetoresistivity in two-dimensional systems induced by Berry curvature, *Phys. Rev. B* **105**, 045421 (2022).
- [14] A. Faridi and R. Asgari, Magnetoresistance in noncentrosymmetric two-dimensional systems, *Phys. Rev. B* **107**, 235417 (2023).
- [15] D. Tu, C. Wang, and J. Zhou, Orbital origin of fourfold anisotropic magnetoresistance in Dirac materials, *Phys. Rev. B* **112**, L041405 (2025).
- [16] H. Rostami and R. Asgari, Valley Zeeman effect and spin-valley polarized conductance in monolayer mos_2 in a perpendicular magnetic field, *Phys. Rev. B* **91**, 075433 (2015).
- [17] A. Knothe and V. Fal'ko, Influence of minivalleys and Berry curvature on electrostatically induced quantum wires in gapped bilayer graphene, *Phys. Rev. B* **98**, 155435 (2018).
- [18] Y. Lee, A. Knothe, H. Overweg, M. Eich, C. Gold, A. Kurzmann, V. Klasovika, T. Taniguchi, K. Wantanabe, V. Fal'ko, T. Ihn, K. Ensslin, and P. Rickhaus, Tunable valley splitting due to topological orbital magnetic moment in bilayer graphene quantum point contacts, *Phys. Rev. Lett.* **124**, 126802 (2020).
- [19] S. Zhong, J. E. Moore, and I. Souza, Gyrotropic magnetic effect and the magnetic moment on the Fermi surface, *Phys. Rev. Lett.* **116**, 077201 (2016).
- [20] Y.-Q. Wang, T. Morimoto, and J. E. Moore, Optical rotation in thin chiral/twisted materials and the gyrotropic magnetic effect, *Phys. Rev. B* **101**, 174419 (2020).
- [21] Y. Gao, S. A. Yang, and Q. Niu, Geometrical effects in orbital magnetic susceptibility, *Phys. Rev. B* **91**, 214405 (2015).
- [22] T. Yamaguchi, K. Nakazawa, and A. Yamakage, Microscopic theory of nonlinear Hall effect induced by electric field and temperature gradient, *Phys. Rev. B* **109**, 205117 (2024).
- [23] K. Nakazawa, T. Yamaguchi, and A. Yamakage, Nonlinear charge and thermal transport properties induced by orbital magnetic moment in chiral crystalline cobalt monosilicide, *Phys. Rev. B* **111**, 045161 (2025).
- [24] D. Xiao, W. Yao, and Q. Niu, Valley-contrasting physics in graphene: Magnetic moment and topological transport, *Phys. Rev. Lett.* **99**, 236809 (2007).
- [25] S. Bhowal and G. Vignale, Orbital Hall effect as an alternative to valley Hall effect in gapped graphene, *Phys. Rev. B* **103**, 195309 (2021).
- [26] K. Das, K. Ghorai, D. Culcer, and A. Agarwal, Nonlinear valley Hall effect, *Phys. Rev. Lett.* **132**, 096302 (2024).
- [27] T. Tanaka, H. Kontani, M. Naito, T. Naito, D. S. Hirashima, K. Yamada, and J. Inoue, Intrinsic spin Hall effect and orbital Hall effect in $4d$ and $5d$ transition metals, *Phys. Rev. B* **77**, 165117 (2008).
- [28] H. Kontani, T. Tanaka, D. S. Hirashima, K. Yamada, and J. Inoue, Giant orbital Hall effect in transition metals: Origin of large spin and anomalous Hall effects, *Phys. Rev. Lett.* **102**, 016601 (2009).
- [29] D. Jo, D. Go, and H.-W. Lee, Gigantic intrinsic orbital Hall effects in weakly spin-orbit coupled metals, *Phys. Rev. B* **98**, 214405 (2018).
- [30] D. Go, D. Jo, C. Kim, and H.-W. Lee, Intrinsic spin and orbital Hall effects from orbital texture, *Phys. Rev. Lett.* **121**, 086602 (2018).
- [31] L. Salemi and P. M. Oppeneer, First-principles theory of intrinsic spin and orbital Hall and Nernst effects in metallic monoatomic crystals, *Phys. Rev. Mater.* **6**, 095001 (2022).
- [32] Y.-G. Choi, D. Jo, K.-H. Ko, D. Go, K.-H. Kim, H. G. Park, C. Kim, B.-C. Min, G.-M. Choi, and H.-W. Lee, Observation of the orbital Hall effect in a light metal Ti , *Nature* **619**, 52 (2023).
- [33] I. Lyalin, S. Alikhah, M. Berritta, P. M. Oppeneer, and R. K. Kawakami, Magneto-optical detection of the orbital Hall effect in chromium, *Phys. Rev. Lett.* **131**, 156702 (2023).
- [34] J.-X. Zhu, *Bogoliubov-de Gennes method and its applications*, Vol. 924 (Springer, 2016).
- [35] M. Z. Hasan and C. L. Kane, Colloquium: Topological insulators, *Rev. Mod. Phys.* **82**, 3045 (2010).
- [36] M. Sato and Y. Ando, Topological superconductors: a review, *Reports on Progress in Physics* **80**, 076501 (2017).
- [37] M. Sato and S. Fujimoto, Majorana Fermions and topology in superconductors, *Journal of the Physical Society of Japan* **85**, 072001 (2016).
- [38] V. Cvetkovic and O. Vafek, Berry phases and the intrinsic thermal Hall effect in high-temperature cuprate superconductors, *Nature Communications* **6**, 6518 (2015).
- [39] J. M. Murray and O. Vafek, Majorana bands, Berry curvature, and thermal Hall conductivity in the vortex state of a chiral p -wave superconductor, *Phys. Rev. B* **92**, 134520 (2015).
- [40] L. Liang, S. Peotta, A. Harju, and P. Törmä, Wave-packet dynamics of bogoliubov quasiparticles: Quantum metric effects, *Phys. Rev. B* **96**, 064511 (2017).
- [41] Z. Wang, L. Dong, C. Xiao, and Q. Niu, Berry curvature effects on quasiparticle dynamics in superconductors, *Phys. Rev. Lett.* **126**, 187001 (2021).
- [42] Z.-Q. Zhou, W. Wang, Z. Wang, and D.-X. Yao, Topological superconducting states and quasiparticle transport on the kagome lattice, *Phys. Rev. B* **108**, 184506 (2023).
- [43] Y. Zhang, D.-X. Yao, and Z. Wang, Topological superconductivity with large Chern numbers in a ferromagnetic-metal-superconductor heterostructure, *Phys. Rev. B* **108**, 224513 (2023).
- [44] Z.-C. Liao, C. Xiao, Z. Wang, and Q. Niu, Berry curvature induced spin Nernst and thermal Edelstein effects in proximity superconductors (2024), arXiv:2412.08451.
- [45] Y. Liao and Y.-T. Hsu, Detecting topological superconductivity via Berry curvature effects in spectral functions, *Phys. Rev. B* **111**, 064508 (2025).
- [46] T.-C. Hsieh, C. Xiao, and Y.-T. Hsu, Intrinsic Nernst effect from Berry curvature in superconductors (2025), arXiv:2509.26638.
- [47] J. F. Annett, B. L. Györfy, and K. I. Wysokiński, Orbital magnetic moment of a chiral p -wave superconductor, *New Journal of Physics* **11**, 055063 (2009).
- [48] J. Robbins, J. F. Annett, and M. Gradhand, Theory of the orbital moment in a superconductor, *Phys. Rev. B* **101**, 134505 (2020).

- [49] C. Xiao and Q. Niu, Conserved current of nonconserved quantities, *Phys. Rev. B* **104**, L241411 (2021).
- [50] W.-Y. He and K. T. Law, Superconducting orbital magnetoelectric effect and its evolution across the superconductor-normal metal phase transition, *Phys. Rev. Res.* **3**, L032012 (2021).
- [51] L. Chirolli, M. T. Mercaldo, C. Guarcello, F. Giazotto, and M. Cuoco, Colossal orbital Edelstein effect in noncentrosymmetric superconductors, *Phys. Rev. Lett.* **128**, 217703 (2022).
- [52] S. Ando, Y. Tanaka, M. Cuoco, L. Chirolli, and M. T. Mercaldo, Spin and orbital Edelstein effect in spin-orbit coupled noncentrosymmetric superconductors, *Phys. Rev. B* **110**, 184503 (2024).
- [53] Z. Zhu, M. Papaj, X.-A. Nie, H.-K. Xu, Y.-S. Gu, X. Yang, D. Guan, S. Wang, Y. Li, C. Liu, J. Luo, Z.-A. Xu, H. Zheng, L. Fu, and J.-F. Jia, Discovery of segmented Fermi surface induced by Cooper pair momentum, *Science* **374**, 1381 (2021).
- [54] D. Phan, J. Senior, A. Ghazaryan, M. Hatefipour, W. M. Strickland, J. Shabani, M. Serbyn, and A. P. Higginbotham, Detecting induced $p \pm ip$ pairing at the al-inas interface with a quantum microwave circuit, *Phys. Rev. Lett.* **128**, 107701 (2022).
- [55] A. Damascelli, Z. Hussain, and Z.-X. Shen, Angle-resolved photoemission studies of the cuprate superconductors, *Rev. Mod. Phys.* **75**, 473 (2003).
- [56] O. Fischer, M. Kugler, I. Maggio-Aprile, C. Berthod, and C. Renner, Scanning tunneling spectroscopy of high-temperature superconductors, *Rev. Mod. Phys.* **79**, 353 (2007).
- [57] Y. Jiang, D.-X. Yao, E. W. Carlson, H.-D. Chen, and J. Hu, Andreev conductance in the $d+id'$ -wave superconducting states of graphene, *Phys. Rev. B* **77**, 235420 (2008).